



Edge eigen-stress and eigen-displacement of armchair molybdenum disulfide nanoribbons



Quan Wu^a, Xi Li^a, Alex A. Volinsky^b, Yanjing Su^{a,*}

^a Corrosion and Protection Center, Key Laboratory for Environmental Fracture (MOE), University of Science and Technology Beijing, Beijing 100083, China

^b Department of Mechanical Engineering, University of South Florida, Tampa, FL 33620, USA

ARTICLE INFO

Article history:

Received 19 September 2016

Received in revised form 23 February 2017

Accepted 6 March 2017

Available online 9 March 2017

Communicated by R. Wu

Keywords:

MoS₂ nanoribbons

Size-dependent

Young's modulus

Poisson's ratio

ABSTRACT

Edge effects on mechanical properties of armchair molybdenum disulfide nanoribbons were investigated using first principles calculations. The edge eigen-stress model was applied to explain the relaxation process of forming molybdenum disulfide nanoribbon. Edge effects on surface atoms fluctuation degree were obtained from each fully relaxed nanoribbon with different width. Changes of the relaxed armchair molybdenum disulfide nanoribbons structure can be expressed using hexagonal perimeters pattern. Based on the thickness change, relaxed armchair molybdenum disulfide nanoribbons tensile/compression tests were simulated, providing intrinsic edge elastic parameters, such as eigen-stress, Young's modulus and Poisson's ratio.

© 2017 Elsevier B.V. All rights reserved.

1. Introduction

Molybdenum disulfide (MoS₂) belongs to two-dimensional (2D) transition metal dichalcogenides [1]. Single layer MoS₂ is constructed by graphene-like hexagonal arrangement of Mo and S atoms stacked together to form S–Mo–S sandwiches. Recently, single layer MoS₂ captured researchers' interest due to its prominent mechanical [2–4], electronic [5], thermal [6], and optoelectronic [7] properties.

MoS₂ nanoribbons (MoS₂ NRs) are MoS₂ strips with ultra-narrow width, obtained using electrochemical methods [8]. Based on their edge configuration, MoS₂ NRs are classified as armchair MoS₂ nanoribbons (AMoS₂ NRs) and zigzag MoS₂ nanoribbons (ZMoS₂ NRs). For armchair graphene ribbons (AGNRs), unique mechanical properties were found where AGNRs exhibited three periodicities in the nominal Young's modulus and Poisson's ratio [25]. Considering their band gap [9], intrinsic carrier mobility [10] and binding energy [11], AMoS₂ NRs exhibit oscillating width-dependent behavior. The authors wanted to figure out whether AMoS₂ NRs exhibit three periodicities in the nominal Young's modulus and Poisson's ratio, and further investigate the reasons. The elastic modulus [10–12], edge energy density [13,14] and edge stress [13,15] have been obtained for MoS₂ NRs considered as 2D

structures, i.e., without taking into account the influence of MoS₂ NRs thickness. However, the thickness of MoS₂ NRs varies with the width change. Hence, it is important to accurately determine the edge properties by taking into consideration the thickness change. Intrinsic edge parameters effects on mechanical properties, surface atoms fluctuation degree, edge eigen-stress and Poisson's ratio need to be investigated.

By taking the stress-free monolayer MoS₂ sheet as a reference, an AMoS₂ NR can be created from it. A newly formed AMoS₂ NR, with the lattice constant of the stress-free monolayer MoS₂ sheet, has substantially higher excess energy, and the free-edges (S–Mo–S sandwich structure) of the AMoS₂ NR are formed with eigen-stress [16]. The newly formed AMoS₂ NR relaxes unavoidably to reduce the excess energy and the edge eigen-stress. This relaxation causes initial deformation and relaxation-induced strain in the AMoS₂ NR along the length and thickness directions.

In the present study, AMoS₂ NRs were allowed to relax in two steps of normal relaxation and parallel relaxation, so that the change in the excess energy could be systematically studied. The surface atoms fluctuation degree was obtained from the changes of atomic positions at two layers of sulfur atoms. Perimeters of each hexagon ring in the relaxed AMoS₂ NRs are given to investigate the structure change. The nominal Young's modulus and Poisson's ratio were determined by performing tensile/compressive tests on the relaxed AMoS₂ NRs to extract the edge eigen-stress, edge Young's modulus and Poisson's ratio.

* Corresponding author.

E-mail addresses: volinsky@usf.edu (A.A. Volinsky), yjsu@ustb.edu.cn (Y. Su).

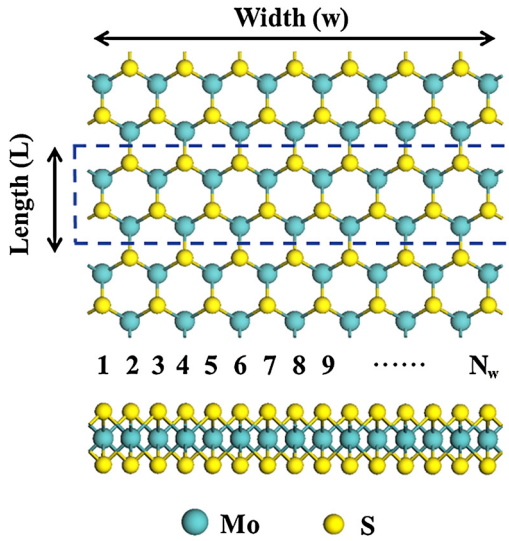


Fig. 1. The calculated geometry of the AMoS₂ NRs.

2. Computational methods

Density functional theory (DFT) calculations were performed by using the Vienna *ab initio* simulation package (VASP) [17] with the project-augmented wave (PAW) method [18]. The exchange correlation interaction was treated by the generalized gradient approximation with the PW91 functional [19]. The PAW potentials were used with the 4p⁶5s¹4d⁵ valence states of molybdenum atoms and the 3s²3p⁴ valence states of sulfur atoms. The 11 × 11 × 1 and 1 × 11 × 1 Monkhorst-Pack [20] *k*-points were set for the monolayer MoS₂ and AMoS₂ NRs, respectively, with an energy cut-off of 550 eV. The accuracy of the total energy calculations was on the order of 0.1 meV.

The equilibrium configuration of the monolayer MoS₂ was determined by energy minimization. The spacing of the nearest Mo–Mo was 3.197 Å, the bond length of the Mo–S bond was 2.421 Å, while the distance between the top and bottom layers in single layer MoS₂ was 3.132 Å, in good agreement with previous reports [21,22]. When an AMoS₂ NR is removed from its stress-free parent sheet, it has original dimensions of $L_0 \times W_0 \times T_0$, where L_0 , W_0 and T_0 represent the length, width and thickness of the AMoS₂ NR without any relaxation, respectively. The unrelaxed AMoS₂ NRs width W_0 was determined by using the equal mass method [23], i.e., the total mass of the atoms in the AMoS₂ NR was set equal to the product of the monolayer MoS₂ density and the volume of the simulated representative nanoribbon in its undistorted configuration. The number of atoms across the ribbon width index N_w was adopted to represent the width in this study, and the calculated AMoS₂ NR width ranged from 1.3 nm to 2.4 nm. The unrelaxed AMoS₂ NRs thickness T_0 was equal to the thickness of the MoS₂ monolayer, assumed to be 0.65 nm [3]. Fig. 1 shows that the structure was treated with periodic boundary conditions along the AMoS₂ NR length. To eliminate the interaction between AMoS₂ NRs, the calculated structure contained two 20 Å thick vacuum layers along the width and thickness directions.

3. Theoretical analysis

The relaxation process of AMoS₂ NR was separated into normal and parallel relaxations [16,25]. In the normal relaxation, all of the atoms were allowed to move in width and thickness directions, whereas in parallel relaxation, all of the atoms were allowed to move in all three directions.

The dimensions changes to $L^{ini} \times W^{ini} \times T^{ini}$ with $L^{ini} = L_0 + \Delta L$, $W^{ini} = W_0 + 2p_0 + \Delta W$ and $T^{ini} = T_0 + \Delta T$, where p_0 is the edge eigen-displacement [22] and the change of width ΔW and thickness ΔT are caused by the Poisson's ratio effect. Relaxation causes initial deformation, and the relaxation-induced strain along the AMoS₂ NRs length and thickness directions are called the initial strain. The initial strain along the length and thickness directions is calculated as $\varepsilon_L^{ini} = (L^{ini} - L_0)/L_0$ and $\varepsilon_T^{ini} = (T^{ini} - T_0)/T_0$.

In equilibrium, zero total force along the length direction must be satisfied along any lateral section perpendicular to the length, and the traction-free boundary conditions must be met along the AMoS₂ NR edges. The initial edge stress and core stress after parallel relaxation were calculated as $\sigma_e^{ini} = \sigma_0^{ini} + Y_e \varepsilon_L^{ini}$ and $\sigma_c^{ini} = Y_c \varepsilon_L^{ini}$, respectively. The self-balanced force requires

$$2F_e^{ini} + F_c^{ini} = 0 \quad (1)$$

where $F_e^{ini} = T^{ini} \sigma_e^{ini} = T^{ini} (\sigma_0^{ini} + Y_e \varepsilon_L^{ini})$ and $F_c^{ini} = W^{ini} T^{ini} Y_c \varepsilon_L^{ini}$ denotes the edge force and the core force, which includes the surface force of the two surfaces (S atomic layer) and the core force (Mo atomic layer) per unit length, respectively.

4. Results and discussion

Fig. 2(b) shows that the initial strain along the length direction increases as the width increases, whereas the initial strain along the thickness direction decreases with the width. As the dimensions change, the structures also change.

The edge effect on surface atoms fluctuation degree R_a of each fully relaxed AMoS₂ NR with different width was proposed to reflect the fluctuations of sulfur atomic layers at zero temperature. It was calculated using $R_a = \frac{1}{n_s} \sum_{i=1}^{n_s} \sqrt{2} [|Z_{top}^{NR} - Z_{top}^{sheet}| + |Z_{bottom}^{NR} - Z_{bottom}^{sheet}|]$, where n_s is the total number of sulfur atoms in AMoS₂ NRs, Z_{top}^{NR} , Z_{bottom}^{NR} , Z_{top}^{sheet} and Z_{bottom}^{sheet} denote the sulfur atomic coordinate value along the thickness direction of the AMoS₂ NR's top-layer, AMoS₂ NR's bottom-layer, sheet's top-layer, and sheet's bottom-layer, respectively. Fig. 2(a) shows that the AMoS₂ NR surface atoms fluctuation degree increases as the width decreases. In this case, the change of thickness ΔT is determined by $\Delta T = d_{S-S}^{NR} - d_{S-S}^{sheet}$ in consideration of the uneven surface, where d_{S-S}^{NR} and d_{S-S}^{sheet} denote the arithmetic mean distance between the top layer and the bottom layer in AMoS₂ NRs and stress-free MoS₂ parent sheet, respectively.

The latest study [25] shows that the armchair graphene nanoribbons (AG NRs) with similar honeycomb-like structure to AMoS₂ NRs exhibit three periodicities in the nominal Young's modulus and Poisson's ratio. Investigations of the Young's modulus and Poisson's ratio of AMoS₂ NRs are reported later in the paper. The phenomenon of the width-dependent elastic properties and perimeter patterns with a periodicity of three depends on the nature of the edge, which can be explained by the Clar sextets [26]. The Clar sextets defined as six π -electrons localized in a single hexagons ring separated from adjacent rings by the C–C single bonds. Corresponding relationships were found between the hexagon perimeter pattern and the Clar sextets in AG NRs [26]. Without the Clar sextets, AMoS₂ NRs exhibit different hexagon perimeter pattern. Fig. 3 shows the hexagon "perimeters" (six sides are not in the same plane) of each relaxed AMoS₂ NRs with width N_w ranging from 8 to 15. In contrast to the AG NRs, the perimeter patterns of the AMoS₂ NRs show different variation rules. For the AMoS₂ NRs with $3n + 1$ and $3n - 1$ width, no obvious arrangement rule was observed. According to the structural symmetry, AMoS₂ NRs were classified by central ($N_w = 2k$) and mirror ($N_w = 2k + 1$) symmetry. As the width increases, the value of the hexagonal perimeter approaches the infinite MoS₂ sheet value.

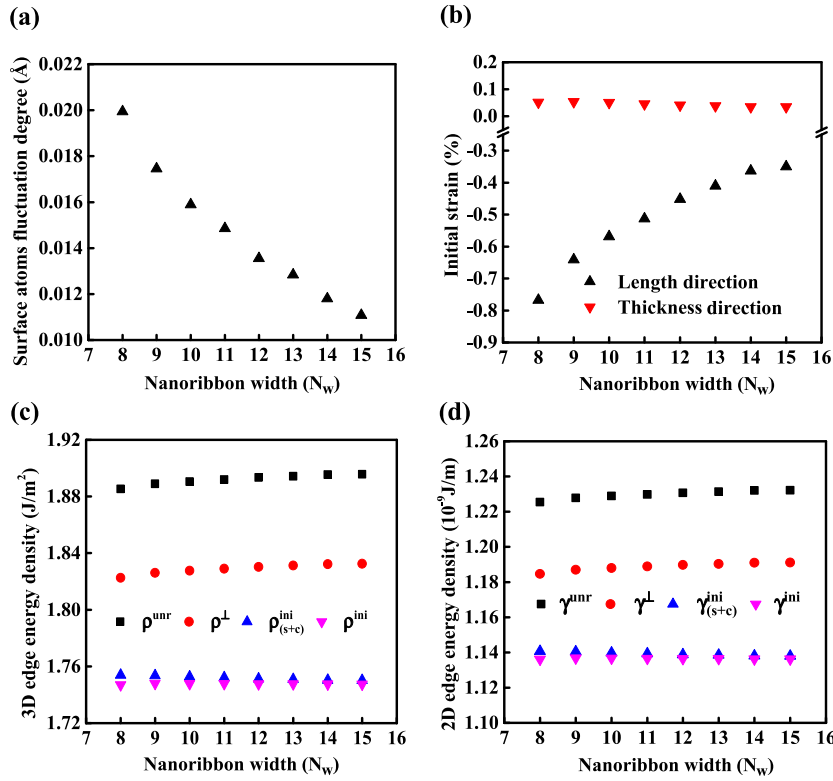


Fig. 2. (a) The surface atoms fluctuation degree; (b) the initial strain; (c) 3D and (d) 2D edge energy densities of AMoS₂ NRs as functions of the width index.

The infinite MoS₂ sheets and MoS₂ NRs are usually treated as a 2D structure to extract their mechanical parameters [3]. However, Fig. 2(b) indicated that around 0.03–0.05% tensile strain forms in the thickness direction of the AMoS₂ NRs during relaxation and deformation, and changes with the width. Hence, AMoS₂ NR is treated as a composite of a geometrical 3D core and two 2D edges to extract its energy change during relaxation, and its mechanical parameters, such as eigen-stress, Young's modulus and Poisson's ratio.

The energy of an AMoS₂ NR without relaxation is calculated from $E^{unr} = E_0 + E_{exc}^{unr}$, where E_0 and E_{exc}^{unr} represent the reference energy of the stress-free monolayer MoS₂ sheet and the unrelaxed excess energy, respectively. E_{exc}^{unr} includes two parts: chemical energy formed due to broken chemical bonds of the edge atoms during the formation of the two nanoribbon edges, and the strain energy of the thickness formed due to transformation from the edge atoms. Thus, the unrelaxed edge energy density is given by $\rho^{unr} = E_{exc}^{unr}/(2L_0T_0^{unr})$, where T_0^{unr} denotes the thickness of the AMoS₂ NRs, which changes with the AMoS₂ NRs width. After normal relaxation, the potential energy decreases from E^{unr} to $E^{\perp r} = E_0 + E_{exc}^{\perp r}$, where $E_{exc}^{\perp r}$ denotes the excess energy after normal relaxation, and the edge energy density decreases to $\rho^{\perp} = E_{exc}^{\perp r}/(2L_0T_0^{\perp})$. Parallel relaxation further reduces potential energy to $E^{ini} = E_0 + E_{exc(e+c)}^{ini}$, where $E_{exc(e+c)}^{ini}$ denotes the total excess energy relative to the stress-free monolayer MoS₂ sheet. Due to the initial deformation, the total excess energy $E_{exc(e+c)}^{ini}$ contains two parts: the core strain energy $E_{exc(c)}^{ini}$, which is equivalent to the strain energy of the sheet counterpart by the relaxation-induced initial deformation and the excess energy attributed to the edge $E_{exc(e)}^{ini}$. The core strain energy E_c^{ini} is determined as $E_c^{ini} = (L^{ini}W^{ini}T^{ini})Y_{3D}^C(\varepsilon_L^{ini})^2$, where ε_L^{ini} denotes the initial strain of the cores along the length and Y_{3D}^C denotes the 3D bulk Young's modulus. Hence, the edge energy density $\rho_{(e+c)}^{ini}$ is calculated from $\rho_{(e+c)}^{ini} = E_{exc(e+c)}^{ini}/(2L^{ini}T^{ini})$ and the edge energy density ρ^{ini} can

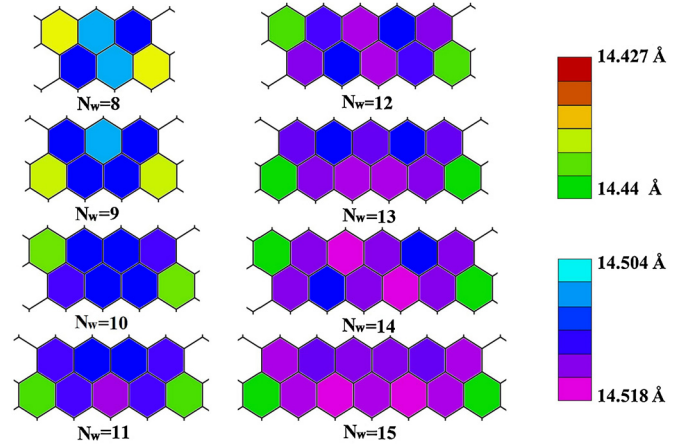


Fig. 3. Hexagon perimeters of each of AMoS₂ NRs with width N ranging from 8 to 15.

be obtained as $\rho^{ini} = E_{exc(e)}^{ini}/(2L^{ini}T^{ini})$. This indicates that under the fully relaxed state in Fig. 2(c), the edge energy density is almost constant when the width index $N > 8$, and slightly lower than the excess energy density. If the AMoS₂ NR is treated as a 2D structure, the corresponding edge energy density above can be defined as $\gamma^{unr} = E_{exc}^{unr}/2L_0$, $\gamma^{\perp} = E_{exc}^{\perp r}/2L_0$, $\gamma_{(e+c)}^{ini} = E_{exc(e+c)}^{ini}/2L^{ini}$, and $\gamma^{ini} = E_{exc(e)}^{ini}/2L^{ini}$, respectively. This indicates in Fig. 2(d) that γ^{unr} and γ^{\perp} increase and $\gamma_{(e+c)}^{ini}$ decreases with the thickness if the change of the AMoS₂ NR thickness during relaxation and deformation is not taken into account. The 2D edge energy density γ^{ini} is almost constant with the increase of the AMoS₂ NRs width.

The simulated uniaxial compression/tensile tests were conducted on the relaxed AMoS₂ NRs and monolayer MoS₂ sheet. A range of 0% to 1% (–1%) uniaxial strain was implemented to adjust the periodic length L with an increment (or decrement)

Table 1
Core and edge Young's modulus, width and thickness directional Poisson's ratio, and eigen-stress of AMoS₂ NRs.

	Young's modulus		Poisson's ratio (width)		Poisson's ratio (thickness)		Eigen-stress
	Core	Edge	Core	Edge	Core	Edge	
3D	187.29 GPa	−29.61 N/m	0.25	0.75 Å	0.11	−0.32 Å	0.71 N/m
2D	121.74 N/m	−19.22 nN	0.25	0.75 Å			0.46 nN

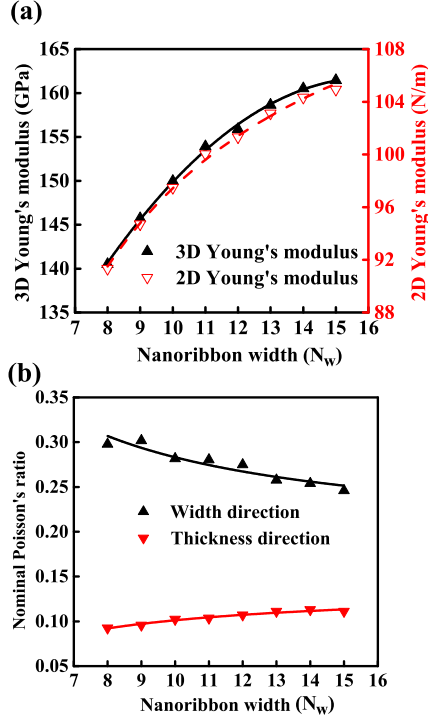


Fig. 4. (a) The uniaxial Young's modulus and (b) Poisson's ratio of the AMoS₂ NRs versus width.

of 0.2%. After each increment (or decrement), energy minimization was conducted to ensure that the simulated system reached a new equilibrium state. Considering the change of thickness, the 3D nominal Young's moduli of the sheet Y_{3D}^{sheet} and nanoribbons Y_{3D}^* were determined as $\Delta U/(L_0 W_0 T_0) = Y_{3D}^{sheet}(\epsilon_L)^2/2$ and $\Delta U/(L^{ini} W^{ini} T^{ini}) = Y_{3D}^*(\epsilon_L)^2/2$, respectively, where ΔU is the strain energy of the nanoribbon and ϵ_L is the applied uniaxial strain. The 2D nominal Young's moduli of the sheet Y_{2D}^{sheet} and nanoribbons Y_{2D}^* can be obtained as $Y_{2D}^{sheet} = T_0 Y_{3D}^{sheet}$ and $Y_{2D}^* = T^{ini} Y_{3D}^*$, respectively. The 3D and 2D Young's moduli of an infinite MoS₂ sheet and nanoribbons are listed in Table 1, and are consistent with the experimentally measured values [2,3].

Fig. 4(a) shows the 3D and 2D nominal uniaxial Young's modulus versus the ribbon width. The nominal Young's modulus of AMoS₂ NRs exhibits width-dependent behavior, i.e., larger width corresponds to higher nominal Young's modulus. The nominal uniaxial Young's modulus is expressed as

$$Y_{3D}^* = Y_{3D}^c + \frac{2Y_{3D}^e}{W} \quad (2)$$

$$Y_{2D}^* = Y_{2D}^c + \frac{2Y_{2D}^e}{W} \quad (3)$$

Both the 3D and 2D edge Young's moduli were calculated by fitting the nominal Young's modulus to the width of the AMoS₂ NRs, and the value of the core Young's modulus is equal to that of the MoS₂ sheet, as listed in Table 1. The negative edge Young's modulus suggests that the nominal uniaxial Young's modulus is lower than the core Young's modulus.

When uniaxial strain ϵ_L^{\parallel} is applied along the length direction, there is a strain ϵ_W^{\perp} along the width direction and ϵ_T^{\perp} along the thickness direction. The perpendicular strains ϵ_W^{\perp} and ϵ_T^{\perp} were available in the simulations, enabling the determination of the width direction nominal Poisson's ratio $v_W^* = -\epsilon_W^{\perp}/\epsilon_L^{\parallel}$ and the thickness direction nominal Poisson's ratio $v_T^* = -\epsilon_T^{\perp}/\epsilon_L^{\parallel}$, for each AMoS₂ NR. Fig. 4(b) shows both the width and thickness directions nominal Poisson's ratio versus the width, indicating that the width direction nominal Poisson's ratio decreased as the width increased, and the thickness direction nominal Poisson's ratio increased as the width increased. Following the edge eigen-displacement model [24] the nominal Poisson's ratios were expressed as

$$v_W^* = v_W^c + \frac{2v_W^e}{W} \quad (4)$$

$$v_T^* = v_T^c + \frac{2v_T^e}{W} \quad (5)$$

where v_W^c , v_W^e and v_T^e are the core, width edge and thickness edge Poisson's ratios, respectively. The edge Poisson's ratios, which represent the excess Poisson's ratio induced by the presence of an edge, are listed in Table 1. The positive value for the width direction Poisson's ratio suggests that the nominal Poisson's ratio decreased as the width increased and was larger than the monolayer sheet width direction Poisson's ratio. The negative value for the thickness direction Poisson's ratio suggests that the nominal Poisson's ratio increased with the width and was smaller than the monolayer sheet thickness direction Poisson's ratio. Periodically modulated width-dependent Young's modulus and Poisson's ratio of AMoS₂ NRs were not observed. The results show that the phenomenon of the width-dependent elastic properties with periodicity of three depends on the nature of the edge, which is not mainly caused by the unique honeycomb-like structure in arm-chair ribbons. Compared with the AG NRs, calculation results in this study indicate that the Clar sextets play the key role in the periodically modulated width-dependent behavior.

From Equation (2), (3) and using Equation (1), the length directional initial strain is treated as a function of the width, which takes the form

$$\epsilon_{3D}^{ini} = \frac{-2\sigma_{0-3D}^{ini}}{W(Y_{3D}^c + \frac{2Y_{3D}^e}{W})} = \frac{-2\sigma_{0-3D}^{ini}}{WY_{3D}^*} \quad (6)$$

$$\epsilon_{2D}^{ini} = \frac{-2\sigma_{0-2D}^{ini}}{W(Y_{2D}^c + \frac{2Y_{2D}^e}{W})} = \frac{-2\sigma_{0-2D}^{ini}}{WY_{2D}^*} \quad (7)$$

The 3D and 2D edge eigen-stresses, listed in Table 1, were determined by fitting the calculated initial strain versus the reciprocal of the product of the width and the nominal Young's modulus. The positive edge eigen-stress suggests that the edges of AMoS₂ NRs are stretched when constructed with the monolayer MoS₂ sheet lattice constant without any deformation. To release the tensile edge eigen-stress, compressive initial strains must be induced during relaxation.

5. Conclusions

In conclusion, energies and mechanical properties of the AMoS₂ NR with bare edges dimensions changed after normal relaxation

and parallel relaxation. As the width increased, the initial strain along the length increased, and the initial strain along the thickness, the surface atoms fluctuation degree and the edge energy density of the relaxed AMoS₂ NRs decreased. The structure change of the relaxed AMoS₂ NRs with bare edges was expressed by the perimeter patterns, which were divided into two periodic groups. Tensile/compressive tests were conducted on the relaxed AMoS₂ NRs to determine the nominal elastic constants. Nominal Young's modulus and nominal Poisson's ratio also illustrated width-dependent behavior, i.e., larger width corresponded to higher nominal Young's modulus, higher nominal Poisson's ratio along the thickness direction, and smaller nominal Poisson's ratio along the width. The edge Young's modulus and Poisson's ratio were calculated based on the edge eigen-stress and eigen-displacement models. The results obtained herein are helpful to aid MoS₂ nanoribbons-based devices design.

Acknowledgements

This study was supported by the National Basic Research Program of China (Grant No. 2012CB937502).

References

- [1] A.K. Geim, I.V. Grigorieva, *Nature* 499 (2013) 419.
- [2] A.C. Gomez, M. Poot, G.A. Steele, H.S.J. Van der Zant, N. Agrait, G.R. Bollinger, *Adv. Mater.* 24 (2012) 772.
- [3] S. Bertolazzi, J. Brivio, A. Kis, *ACS Nano* 5 (2011) 9703.
- [4] G. Casillas, U. Santiago, H. Barrón, D. Alducin, A. Ponce, M.J. Yacamán, *J. Phys. Chem. C* 119 (2015) 710.
- [5] W.Z. Wu, L. Wang, Y.L. Li, F. Zhang, L. Lin, S. Niu, D. Chenet, X. Zhang, Y.F. Hao, T.F. Heinz, J. Hone, Z.L. Wang, *Nature* 514 (2014) 470.
- [6] X.J. Liu, G. Zhang, Q.X. Pei, Y.W. Zhang, *Appl. Phys. Lett.* 103 (2013) 133113.
- [7] Q.H. Wang, K.K. Zadeh, A. Kis, J.N. Coleman, M.S. Strano, *Nat. Nanotechnol.* 7 (2012) 699.
- [8] Q. Li, J.T. Newberg, E.C. Walter, J.C. Hemminger, R.M. Penner, *Nano Lett.* 4 (2004) 277.
- [9] C. Ataca, H. Sahin, E. Akturk, S. Ciraci, *J. Phys. Chem. C* 115 (2011) 3934.
- [10] Y.Q. Cai, G. Zhang, Y.W. Zhang, *J. Am. Chem. Soc.* 136 (2014) 6269.
- [11] Y.F. Li, Z. Zhou, S.B. Zhang, Z.F. Chen, *J. Am. Chem. Soc.* 130 (2008) 16739.
- [12] J.W. Jiang, H.S. Park, T. Rabczuk, *J. Appl. Phys.* 114 (2013) 064307.
- [13] Z.N. Qi, P.H. Cao, H.S. Park, *J. Appl. Phys.* 114 (2013) 163508.
- [14] H. Pan, Y.W. Zhang, *J. Mater. Chem.* 22 (2012) 7280.
- [15] J. Deng, I. Fampiou, J.Z. Liu, A. Ramasubramaniam, N.V. Medhekar, *Appl. Phys. Lett.* 100 (2012) 251906.
- [16] T.Y. Zhang, Z.J. Wang, W.K. Chan, *Phys. Rev. B* 81 (2010) 195427.
- [17] G. Kresse, D. Joubert, *Phys. Rev. B* 59 (1999) 1758.
- [18] P.E. Blöchl, *Phys. Rev. B* 50 (1994) 17953.
- [19] J.P. Perdew, J.A. Chevary, S.H. Vosko, K.A. Jackson, *Phys. Rev. B* 46 (1992) 6671.
- [20] H.J. Monkhorst, J.D. Pack, *Phys. Rev. B* 13 (1976) 5188.
- [21] Q. Peng, S. De, *Phys. Chem. Chem. Phys.* 15 (2013) 19427.
- [22] H. Peelaers, C.G. Van de Walle, *J. Phys. Chem. C* 118 (2014) 12073.
- [23] V.B. Shenoy, *Phys. Rev. B* 71 (2005) 094104.
- [24] T.Y. Zhang, H. Ren, Z.J. Wang, S. Sun, *Acta Mater.* 59 (2011) 4437.
- [25] X. Li, T.Y. Zhang, Y.J. Su, *Nano Lett.* 15 (2015) 4883.
- [26] E. Clar, *The Aromatic Sextet*, Wiley, London, 1972.